TAO, Vol. 9, No. 4, 755-778, December 1998

Active Tectonics of Taiwan Orogeny From Focal Mechanisms of Small-to-moderate-sized Earthquakes

Ruey-Juin Rau[1] and Francis T. Wu[2]

(Manuscript received 29 December 1997, in final form 27 October 1998)

ABSTRACT

We use the focal mechanisms of 97 small-to-moderate-sized earthquakes ($2.7 \leq M_L \leq 5.7$) given by a comprehensive focal mechanism study from Rau *et al.* (1996) to determine the style of faulting and the state of stress in the active Taiwan orogen. The nature of faulting of the 97 minor earthquakes is characterized by a mixture of reverse, normal, and strike-slip faults. Thirty of the 97 events studied are reverse faulting events; 24 of them occurred under the Western Foothills and the Central Range, mostly within a depth range of 10-32 km and a dip angle range of 30-70°. The steeply dipping nodal planes and their deep focal depths demonstrate that the reverse faulting is not confined above a detachment surface, but occurs in the crystalline basement at high angles. Normal faulting events are observed under the northern Central Range in both upper and lower crustal levels and under the Western Foothills in the upper crustal level. The shallow normal faulting under the northern Central Range is probably associated with the uparching of the core of the orogen, causing the vertical stress to be greater under the orogen than under the lowlands. The cause of the deep normal faulting under the Central Range is enigmatic. In the Western Foothills, under the flank of the Central Range, the shallow normal faulting may also be a result of the uparching of the core of the orogen, while the deep reverse faulting is caused by the horizontal compression. The stress tensors estimated are heterogeneous throughout the entire Taiwan region, with the exception of south-central Taiwan where a nearly homogeneous stress field is observed. Although the spreads of the 95% confidence region for σ_1 and σ_3 are relatively large for most stress models, they are consistent with the direction of the plate motion of the Philippine Sea plate relative to the Eurasian plate.

(Key words: Orogeny, Focal mechanism, Stress inversion)

[1]Institute of Earth Sciences, Academia Sinica, Taipei, Taiwan, ROC
[2]Department of Geological Sciences, State University of New York at Binghamton, New York, USA

1. INTRODUCTION

The collision-induced Taiwan orogeny started about 4 m.y.b.p. (Wu, 1978) and is seismically very active. Most large earthquakes ($m_b > 6$) in the Taiwan region have occurred offshore from the east coast or under the eastern part of the island, where northward subduction and the collision of the Philippine Sea plate with the Eurasian continent are taking place (Figures 1 and 2). In central and western Taiwan, the seismicity is dominated by $m_b < 4.5$ events, although the seismicity under the Central Range of Taiwan (at an average elevation of 3000 m) is quite low (Wu *et al.*, 1997). Since large earthquakes have rarely occurred under the Central Range, the study of focal mechanisms of minor earthquakes under this active orogen is likely to be one of the best approaches to understanding the mechanics of modern mountain building, as the earthquakes are responses to the deformation within the orogen. While large earthquakes have been most effective in delineating motions of plates and major intraplate deformation, they are much less frequent and may mask the complexities of source structures making it difficult to unravel them (Kikuchi and Kanamori, 1982). For small to moderate earthquakes ($2.5 < m_b < 5$), the dimensions of the corresponding faults are in the order of 10's of meters to a kilometer (Slemmons and Depolo, 1986; Wells and Coppersmith, 1994); large number of similar mechanisms in an area probably signifies a major structure, while a variety of mechanisms may indicate deformation in a highly fractured medium.

Previously, focal mechanism studies of small-to-moderate-sized earthquakes in the Central Range or the Western Foothills were based on first motions of *P* waves recorded by an earlier telemetered seismic network or temporary portable networks (e.g., Lin and Tsai, 1981; Lee, 1983; Lin and Roecker, 1993). Among these studies, Lin and Roecker (1993) investigated the relation between seismicity/focal mechanisms and tectonics under the northern Central Range in an area around latitude 24°N. They found that the focal mechanisms for nearly all the events with focal depths > 35 km are normal with downdip T axes. Furthermore, they attributed the anomalously deep (> 60 km) Central Range earthquakes to the eastward motion of the Eurasian mantle north of 24°N, which juxtaposes it against colder subducted crust to the south. Furthermore, Kao *et al.* (1998) utilized 62 recent earthquakes of $5.5 \leq m_b \leq 6.6$ occurring in the region between Taiwan and the southernmost Ryukyu arc to investigate the collision and subduction processes taking place there. Other than their work, there have been few other attempts to utilize focal mechanisms to explore the complex relationship between focal mechanisms and the crustal deformation associated with the young Taiwan orogeny.

This study utilizes the results from a comprehensive regional network focal mechanism study (Rau *et al.*, 1996), where *P* wave first motion and *SH/P* amplitude ratio were used to determine 97 focal mechanism solutions ($2.7 \leq M_L \leq 5.7$) at a depth range of 3 - 43 km and within a time period of three and a half years. Although the time period of coverage is very short, the quantity and quality of these results are sufficient to elucidate the deformation and stress patterns associated with the Taiwan orogeny. In this paper, we use these focal mechanisms to discuss two aspects of the orogeny: (1) the style of deformation associated with recognizable seismicity patterns and known surface faults and their association with the orogenic process, and (2) the state of stress in different parts of the Taiwan orogen. The focal mechanisms of large earthquakes ($m_b > 6$) often show a pattern coherent with the principal

regional stress directions. However, the mechanisms of smaller earthquakes often vary, and they probably represent internal deformation of the blocks bounded by larger faults and may not be a reliable regional stress indicator (e.g., England and Jackson, 1989). In spite of the differences in the type of faulting among these mechanisms, the stress tensor can still be inverted with some assumptions. Previously, the regional stress tensors in the Taiwan region were determined by using focal mechanism data resulting from *P* wave first motions (Yeh *et al.*, 1991). Although spatial coverage of the data may be poor, the stress tensors they obtained are consistent with the plate motion vectors in the vicinity of Taiwan (Seno *et al.*, 1993). In the present study the stress field is inverted in different parts of the Taiwan orogen. This may allow us to investigate the spatial variation of the regional stress field within the Taiwan orogen.

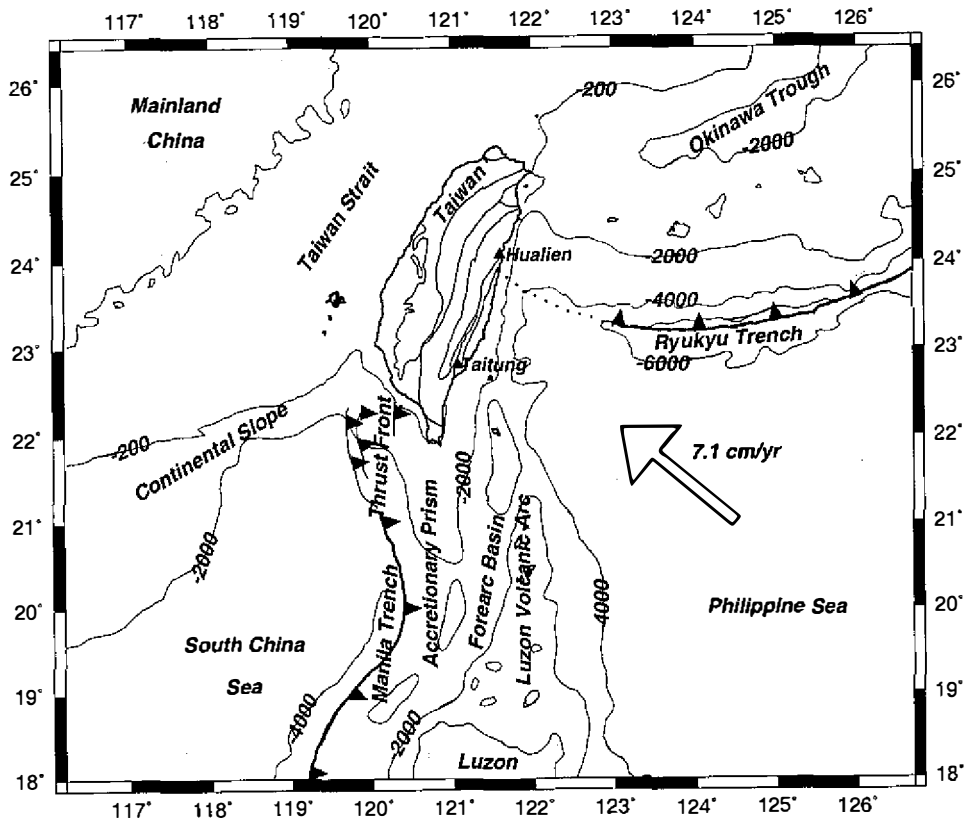

Fig. 1. Bathymetry and tectonic setting of Taiwan and surrounding area (modified from Rau and Wu (1995)). Locations of Ryukyu Trench to east and Manila Trench to south are indicated. Arrow shows vector of relative motion between Philippine Sea plate and Eurasian plate (Seno *et al.*, 1993). Isobaths (in meters) outline morphology of Chinese continental shelf, slope and other features.

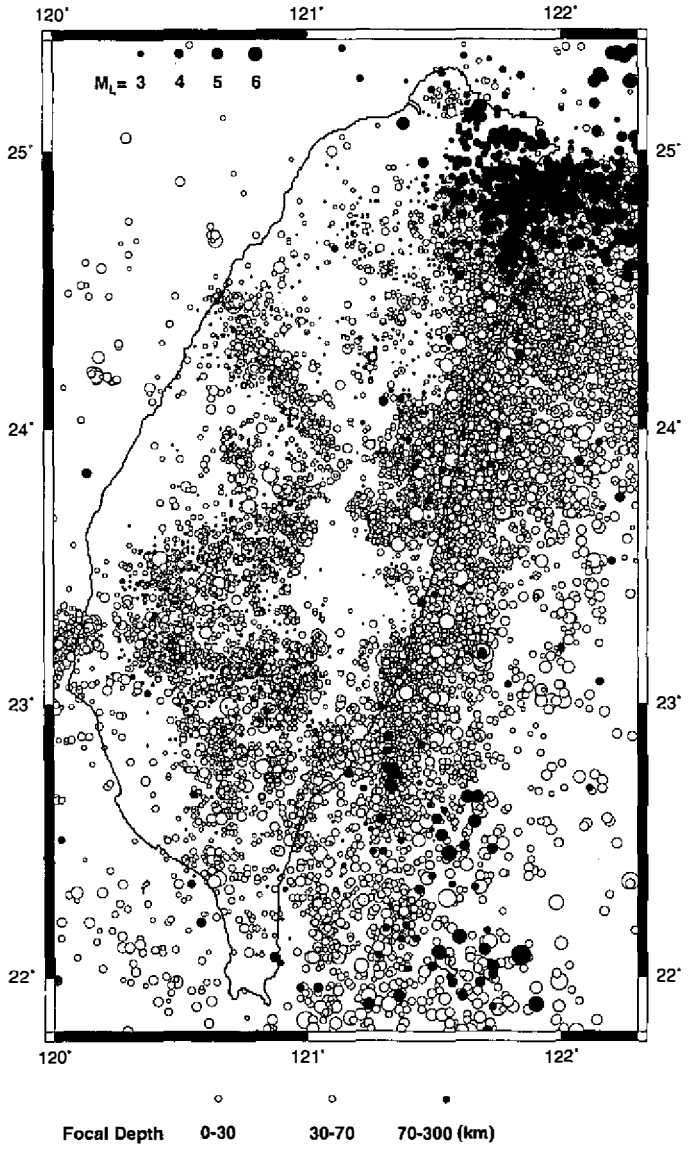

Fig. 2. Seismicity of Taiwan from January 1, 1991 to July 31, 1994. Earthquakes are coded for both magnitude (scale at upper left) and depth (scale at bottom in km).

2. FOCAL MECHANISM DATA

In 1991, the Taiwan seismic network was upgraded from a mostly single component, 25-station telemetered network (Taiwan Telemetered Seismic Network, TTSN; Wang, 1989) to the digitally transmitted three-component 75-station Taiwan Seismic Network (TSN; Figure 3; Shin, 1993). Inter-station spacing has been significantly reduced from about 30-50 km for TTSN to about 10 to 30 km for TSN. The improvement in the dynamic range (from about 40 db to 66 db) in the recording system resulted in a rapid accumulation of high quality waveform data. Thus, studies of both the velocity structures and the focal mechanisms of small to mod-

erate earthquakes become possible. Rau and Wu (1995) used travel time data from the new network to determine a 3-D velocity model under the island. The concurrent relocation for selected events improved the hypocenters considerably. By incorporating *SH/P* amplitude ratio with the first motions in the focal mechanism determination, Rau *et al.* (1996) obtained 97 well-constrained solutions for small to moderate events ($2.7 \leq M_L \leq 5.7$) within a depth range of 3 - 43 km. Compared to those hypocenters using layered half-space and *P* wave polarities only, these new solutions have fewer inconsistencies and are better constrained. The focal mechanisms are listed in Table 1 and plotted in Figure 4a-c.

3. NATURE OF FAULTING IN DIFFERENT REGIONS

Focal mechanisms of the selected 97 earthquakes show a mixure of strike-slip, reverse and normal faulting mechanisms and vary widely under the whole region studied. In order to facilitate discussion we will discuss our focal mechanisms by exploring their relations with seismicity patterns in different areas, with known structures, and with tectonics and stress axes.

To display the 97 solutions in terms of fault types, we plot the mechanisms as points in a ternary diagram (Figure 5a-d; Frohlich, 1992, 1995; Frohlich and Apperson, 1992). In the

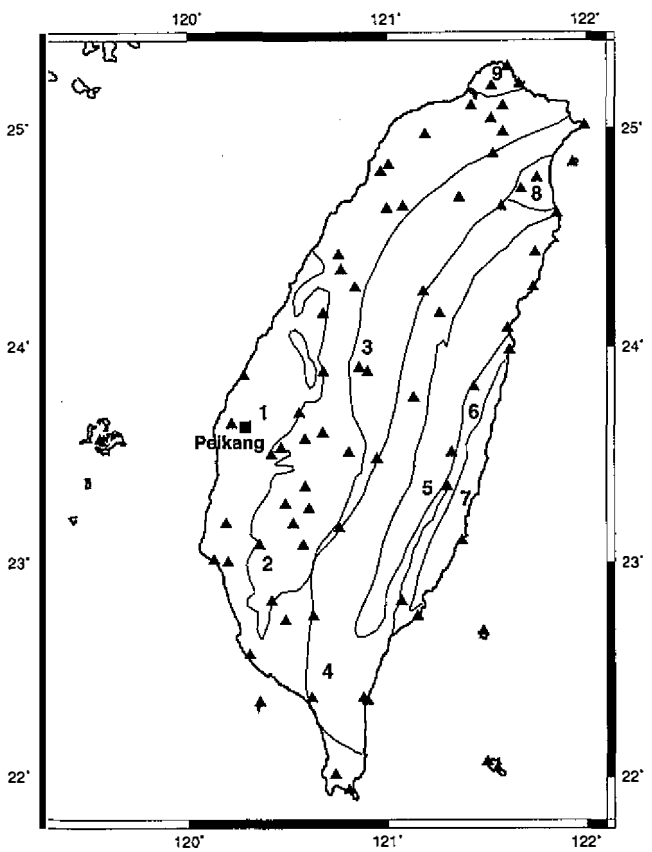

Fig. 3. Map of Taiwan showing locations of 75 seismic stations (solid triangles). Geologic provinces of Taiwan are: 1 - Coastal Plain, 2 - Western Foothills, 3 - Hsuehshan Range, 4 - Backbone Ridge, 5 - eastern Central Range, 6 - Longitudinal Valley, 7 - Coastal Range, 8 - Ilan Plain, 9 - Tatun volcano group; they are separated by solid lines.

Table 1. Source parameters of 97 earthquakes used in this study.

NO	yrmoday	hrmin	lat(N)	lon(E)	depth	mag	Plane 1(s,d,r)	Plane 2(s,d,r)	P(t,p)	T(t,p)	B(t,p)
A1	910405	10:07	24.2	120.88	12.75	3.11	337 56 53	211 48 132	93 4	190 60	0 30
A2	910806	17:31	23.87	120.77	27.17	4.07	326 56 53	199 48 132	81 4	178 60	348 30
A3	910819	06:14	24.35	120.91	26.34	3.32	326 71 -24	64 67 -160	284 30	16 3	110 60
A4	910819	10:44	24.11	120.91	37.44	3.78	22 51 -8	118 84 -140	348 32	243 22	125 50
A5	910906	19:20	23.99	121.02	16.18	3.55	150 20 90	330 70 90	60 25	240 65	150 0
A6	911019	00:00	23.77	120.92	29.36	3.36	343 66 33	238 61 152	109 3	202 40	16 50
A7	911029	08:21	23.82	120.75	16.64	4.41	207 72 64	85 32 144	317 23	84 55	216 25
A8	911218	19:33	23.94	121.13	32.54	3.48	2 16 71	201 75 95	287 30	119 60	20 5
A9	920128	17:23	24.19	120.89	12.88	3.25	309 74 37	207 54 160	74 13	174 37	329 50
A10	920226	08:49	23.84	121.09	26.2	3.56	311 15 0	221 90 105	297 43	146 43	41 15
A11	920227	11:45	24.67	121.2	9.37	3.35	12 59 -16	111 76 -148	336 33	238 11	132 55
A12	920320	21:12	24.58	121.31	5.89	3.01	215 41 -41	338 64 -124	202 57	92 13	354 30
A13	920321	21:07	24.26	120.88	27.34	3.26	223 65 84	56 25 102	317 20	122 69	225 5
A14	920420	16:16	24.44	120.74	11.19	5.19	165 71 -74	304 25 -128	98 61	243 24	339 15
A15	920420	16:31	24.45	120.76	11.52	2.87	323 60 19	223 73 149	275 9	179 34	18 55
A16	920420	16:33	24.44	120.75	10.94	3.47	136 80 -75	258 18 -147	64 52	213 34	314 15
A17	920420	16:48	24.44	120.74	11.23	3.41	178 52 71	27 42 113	282 5	29 74	190 15
A18	920421	13:36	24.44	120.76	11.86	4.58	152 61 6	59 85 150	109 17	11 24	230 60
A19	920422	07:55	24.44	120.75	10.55	3.89	10 60 90	190 30 90	100 15	280 75	10 0
A20	920422	19:59	24.44	120.75	11.17	3.33	137 64 -24	238 68 -152	98 35	6 3	272 55
A21	920426	13:59	24.44	120.76	10.95	3.94	354 41 41	231 64 124	297 13	187 57	35 30
A22	920429	16:54	24.44	120.76	11.56	4.05	178 52 71	27 42 113	282 5	29 74	190 15
A23	920618	20:18	24.22	120.96	30.98	3.05	35 25 -52	175 71 -106	61 61	277 24	180 15
A24	920917	10:41	24.21	120.89	13.49	3.09	289 35 -42	55 67 -117	287 58	165 18	66 25
A25	921216	12:29	24.29	120.84	27.73	4.43	168 86 55	72 35 173	287 32	46 39	171 35
A26	921216	19:11	23.87	120.75	25.8	3.17	336 61 73	189 33 118	79 14	211 69	345 15
A27	921223	18:43	24.17	120.21	29.7	4.27	116 62 -49	235 48 -141	77 54	179 8	275 35
A28	930120	20:21	24.33	120.79	12.69	3.16	342 81 -34	77 56 -170	294 30	34 17	149 55
A29	930122	04:51	24.46	121.41	7.26	3.32	262 70 -85	67 21 -104	181 65	348 25	80 5
A30	930203	08:35	24.27	120.76	10.49	3.38	340 25 52	201 71 106	279 24	134 61	15 15
A31	930208	22:35	24.21	120.77	23	3.3	201 73 42	95 50 157	323 14	66 42	219 45
A32	930319	02:50	24.27	121.13	9.74	3.48	287 61 -78	85 31 -109	224 72	9 15	101 10
A33	930327	14:08	24.3	120.88	31.01	3.19	159 59 16	60 76 148	113 11	16 33	220 55
A34	930504	11:16	24.2	121.01	36.06	3.28	205 69 -58	325 38 -144	156 54	271 17	12 30
A35	930519	13:56	24.06	120.69	20.59	3.25	47 51 77	247 41 105	147 5	263 79	56 10
A36	930602	10:58	24.23	120.9	28.21	3.43	313 85 -80	69 11 -154	234 49	34 39	132 10
A37	930628	12:26	23.77	120.78	23.52	4.07	352 29 58	207 66 106	285 19	146 65	21 15
A38	930810	15:24	24.1	121.01	25.92	4.1	210 71 69	80 28 137	316 23	91 58	217 20
A39	931011	14:01	24.14	121.14	42.07	3.47	7 71 36	264 56 157	133 10	231 38	31 50
A40	931105	17:24	23.88	120.72	12.58	3.4	263 60 -55	28 45 -135	224 59	329 9	64 30
A41	931213	09:23	24.2	120.8	23.4	4.46	177 76 5	86 85 166	132 6	41 14	246 75
A42	931213	09:25	24.2	120.8	22.69	3.22	172 76 21	76 70 165	303 4	35 25	204 65
A43	940210	20:54	24.26	121.24	7.46	3.66	355 55 -90	175 35 -90	265 80	85 10	175 0
A44	940210	20:55	24.25	121.23	8.28	3.28	179 30 -80	347 60 -96	242 74	81 15	350 5
A45	940213	13:14	23.86	120.96	25.96	3.31	258 11 -26	14 85 -100	274 49	114 39	15 10
A46	940220	13:24	23.89	120.73	13.37	3.8	234 21 -44	6 76 -106	256 57	109 29	10 15
A47	940220	14:28	23.89	120.72	12.97	3.54	257 57 -66	38 40 -122	216 68	330 9	64 20
A48	940306	06:44	23.89	120.74	12.61	3.75	228 90 80	138 10 -180	328 44	128 44	228 10
A49	940306	06:46	23.88	120.75	12.69	3.97	29 85 -80	145 11 -154	310 49	110 39	208 10
A50	940306	13:07	23.87	120.72	13.28	3.03	354 47 -69	145 47 -111	339 75	69 0	159 15

NO	yrmoday	hrmin	lat(N)	lon(E)	depth	mag	Plane 1(s,d,r)	Plane 2(s,d,r)	P(t,p)	T(t,p)	B(t,p)
A51	940318	07:32	23.88	120.75	13.08	3.63	228 90 80	138 10 -180	328 44	128 44	228 10
A52	940617	05:31	23.86	120.96	25.59	3.91	313 25 35	191 76 111	264 28	126 54	5 20
A53	940621	23:54	24.03	120.98	15.99	3.55	318 36 31	202 73 122	268 21	149 52	12 30
A54	940629	03:26	24.1	121.07	41.29	3.16	18 79 44	277 47 165	140 21	247 38	28 45
B1	911222	21:35	23.63	120.61	14.64	3.49	181 85 30	88 61 174	311 17	49 24	190 60
B2	911224	02:51	23.19	120.71	13.84	4.92	12 51 77	212 41 105	111 5	227 79	20 10
B3	920204	10:05	23.15	120.41	19.43	4.65	305 66 39	197 55 150	69 7	166 44	332 45
B4	920525	15:55	23.22	120.55	16.85	3.66	144 71 74	5 25 128	246 24	30 61	149 15
B5	920824	18:37	23.56	120.68	13.15	4.71	112 55 84	302 35 99	206 10	359 79	115 5
B6	921122	14:25	23.35	120.66	14.99	4.11	169 50 23	64 73 138	121 14	19 42	226 45
B7	921215	19:11	23.16	120.63	9.46	3.94	335 88 5	245 85 178	110 2	200 5	0 85
B8	930119	10:35	23.44	120.45	11.07	4.26	159 50 4	66 87 140	120 24	15 30	243 50
B9	930321	20:04	23.41	120.62	11.75	3.38	304 82 -18	37 72 -171	260 19	352 7	101 70
B10	930416	21:10	23.18	120.82	5.35	4.87	160 88 5	70 85 178	295 2	25 5	180 85
B11	930424	08:05	23.19	120.81	5.7	3.87	186 41 41	63 64 124	129 13	18 57	226 30
B12	930425	22:14	23.13	120.68	5.91	4.4	144 85 19	52 71 175	277 10	10 17	158 70
B13	930503	16:35	23.36	120.54	12.71	3.59	358 41 75	198 51 103	279 5	163 79	10 10
B14	930503	16:44	23.36	120.54	12.96	3.76	3 56 78	204 36 107	102 10	236 76	10 10
B15	930816	16:37	23.29	120.19	16.35	4.69	301 69 -22	39 69 -158	260 30	350 0	80 60
B16	930816	17:11	23.29	120.19	14.3	4.4	119 87 35	27 55 177	247 22	349 26	123 55
B17	930817	12:46	23.3	120.18	18.72	4.26	296 76 -21	32 70 -165	253 25	345 4	84 65
B18	930919	18:35	23.43	120.49	6.05	4.13	18 35 81	208 55 96	294 10	141 79	25 5
B19	931126	19:22	22.86	120.65	17.65	4.78	192 56 53	66 48 132	307 4	45 60	215 30
B20	931203	10:23	23.51	120.93	7.13	3.88	132 54 -37	247 61 -138	103 50	8 4	275 40
B21	931215	21:49	23.21	120.52	13.88	5.7	205 45 83	35 45 97	120 0	30 85	210 5
B22	931217	02:00	23.54	120.92	4.62	4.23	160 88 5	70 85 178	295 2	25 5	180 85
B23	931217	02:31	23.54	120.92	4.82	4.39	145 64 -24	246 68 -152	107 35	15 3	281 55
B24	931217	20:27	23.54	120.92	6.49	3.53	332 80 -39	70 52 -168	284 34	27 19	141 50
B25	931221	03:14	23.21	120.52	14.96	4.49	106 85 80	350 11 154	205 39	4 49	106 10
B26	931222	16:22	23.22	120.51	15.02	4.63	318 78 28	222 63 166	88 10	183 28	340 60
B27	940103	09:12	23.41	120.53	6.98	4.35	35 60 35	286 60 145	341 0	251 45	71 45
B28	940306	05:47	23.14	120.83	3.46	4.29	343 79 -17	76 74 -168	299 20	30 3	130 70
B29	940328	08:11	22.97	120.67	18.92	5.41	286 60 3	194 88 150	244 19	146 23	10 60
B30	940406	01:12	23.52	120.43	16.15	5.03	159 55 -3	251 87 -145	120 26	19 22	255 55
B31	940617	01:10	23.26	120.59	11.19	3.94	351 85 30	258 61 174	121 17	219 24	0 60
B32	940703	23:28	23.72	120.49	21.87	2.82	279 60 -19	19 73 -149	242 34	146 9	44 55
B33	940724	04:29	23.5	120.53	14.5	3.22	353 76 43	250 48 161	115 17	220 40	7 45
C1	911205	15:48	22.71	121.35	25.44	5.24	17 16 60	228 76 98	312 31	149 58	46 8
C2	920316	19:00	22.79	121.06	10.71	3.17	204 27 20	96 81 115	165 31	33 48	271 25
C3	920510	22:45	22.88	121.08	14.93	3.72	338 61 42	224 54 143	100 4	194 50	7 40
C4	920526	23:19	23.13	121.3	11.98	4.19	191 41 75	31 51 103	112 5	356 79	203 10
C5	920528	20:46	23.16	121.28	4.32	3.39	302 70 52	188 42 149	59 16	170 50	317 35
C6	930305	06:57	22.26	121.03	14.44	5.46	177 51 -34	290 64 -136	150 49	51 8	314 40
C7	930330	17:30	22.86	121.27	16.71	3.59	173 21 13	71 85 110	143 37	1 46	249 20
C8	930428	08:54	22.94	121.25	12.86	3.47	128 45 -45	254 60 -125	112 59	8 9	273 30
C9	930509	02:00	23.04	121.35	18.77	3.39	130 20 90	310 70 90	40 25	220 65	130 0
C10	940506	17:39	22.83	121.09	14.58	3.76	171 75 -13	264 77 -164	128 20	37 2	302 70

(Table 1. continued)

diagram, the pure reverse, pure strike-slip, and pure normal mechanisms are plotted at the apexes of the triangle. For a pure reverse fault dipping at 45°, the dip angle of the T (tension) axis, δ_T, is 90°; for a vertical pure strike-slip fault, the dip of the B (intermediate) axis, δ_B is 90°; and for a 45° normal fault, the dip of the P (pressure) axis, δ_P is 90°. Along the axis opposite an apex, such as $\delta_B = 90°$, the dip angle is 0 (here, $\delta_B = 0°$). For any mechanism, the three dip angles satisfy the following relation:

$$\sin^2\delta_T + \sin^2\delta_B + \sin^2\delta_P = 1. \quad (1)$$

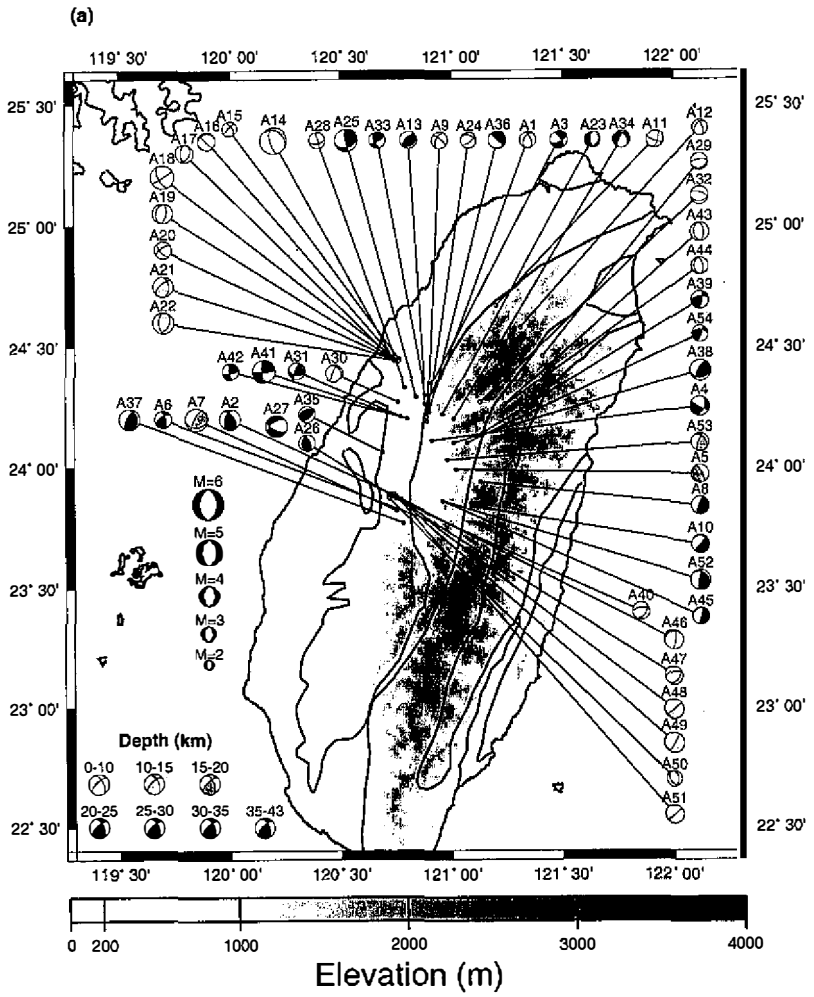

Fig. 4. Focal mechanisms of 97 events studied. (a) 54 events for north-central Taiwan (b) 33 events for south-central Taiwan (c) 10 events for south-eastern Taiwan.

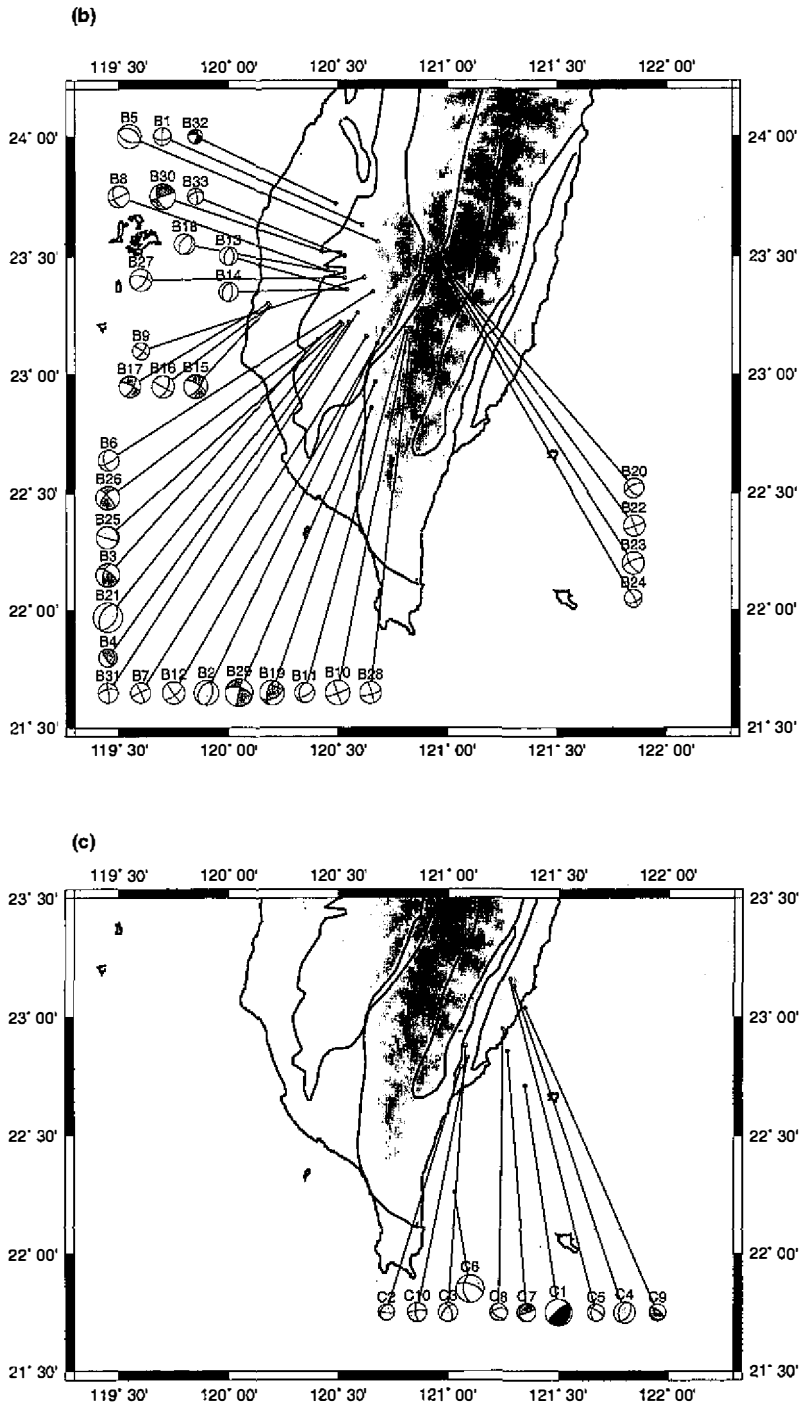

(*Fig. 4.* continued)

The actual mechanisms are plotted as points in the interior. Following Frohlich and Apperson (1992), we define an earthquake as normal or strike-slip if δ_P or δ_B, respectively, exceeds 60°, and reverse if δ_T exceeds 50°. All other event-types are designated as "odd".

In addition to discussing the mechanisms of this region as a whole, we divided the data into three subsets — north-central, south-central, and southeastern Taiwan — to examine the stress inversion and the characterization of fault types. The division was based on tectonic setting and the distribution of seismicity (Figures 2 and 3). The separation between north-central and south-central Taiwan is the Peikang basement high.

3.1 The Whole of Taiwan

On the ternary diagram of the 97 mechanisms for the whole of Taiwan (Figure 5a), there are 30 reverse, 8 normal, 17 strike-slip, and 42 odd mechanisms. Three noticeable elements can be extracted from Figure 5a: (1) 17 of the 30 events with reverse faulting mechanisms were located in the Western Foothills; (2) 7 of the 8 events with normal faulting mechanisms occurred under the Central Range; and (3) 10 of the 17 events with strike-slip faulting mechanisms were located in the Western Foothills. The depth ranges are 4-42 km, < 14 km (7 of the 8 events), and 3-26 km for the reverse, normal, and strike-slip faulting mechanisms, respectively.

3.2 North-central Taiwan

Of the 54 focal mechanisms in north-central Taiwan (Figure 4a), 26 of them fall into the odd mechanism sector on the ternary diagram (Figure 5b). About one-third (16) of the mechanisms belong to the reverse faulting regime, 8 to the normal, and only 4 to the strike-slip. Based on the separation of the tectonic region, 7 of the 8 normal faulting mechanisms were located under the Central Range, and 6 of these have depths < 14 km. Of the 16 events that fall into the reverse faulting sector, 11 of them are in the Western Foothills, and 5 are in the Central Range. These events have a depth range of 10-32 km.

There are 35 focal mechanisms from events within the NW-SE linear seismic zone in the north-central Taiwan (Figure 2). This zone was identified as the Sanyi Transfer Fault Zone by a geomorphic study (Deffontaines *et al.*, 1994). The mechanisms and their P and T orientations in this zone vary widely, and it is not possible to relate the seismicity pattern to the style of faulting we obtained in this study.

The normal faulting events observed in the northern Central Range (between latitude 24.3 and 24.6°N) have T-axes trending either E-W (A12, A23, A43, A44) or N-S (A29, A32). The shallow normal faulting earthquakes occurred adjacent to the boundary between the Hsuehshan Range and the Backbone Range - the Lishan fault. The fault is a major geologic break in the northern Central Range, but its structural nature remains unclear (Biq, 1971; Chen *et al.*, 1983; Teng *et al.*, 1991; Clark *et al.*, 1993; Lee *et al.*, 1997). Note that from field investigations (Crespi *et al.*, 1996) there are late-stage brittle normal faults observed east of the Lishan fault, where some of our shallow events with normal faulting mechanisms occurred. At deeper levels (~33 km) two normal faulting earthquakes (A23, A34) occurred. Although A34 was not classified as a normal fault in the ternary diagram, it contains a large normal component.

The April 20, 1992 event (A14, M_L = 5.2) has a normal faulting mechanism; the nodal planes are oriented NNW-SSE, dipping either gently to the NNE or steeply to the SSW. The mechanisms of the 8 larger aftershocks (A15-22) accompanying event A14 appear to be complicated and exhibit a mixture of strike-slip, reverse and normal faulting mechanisms.

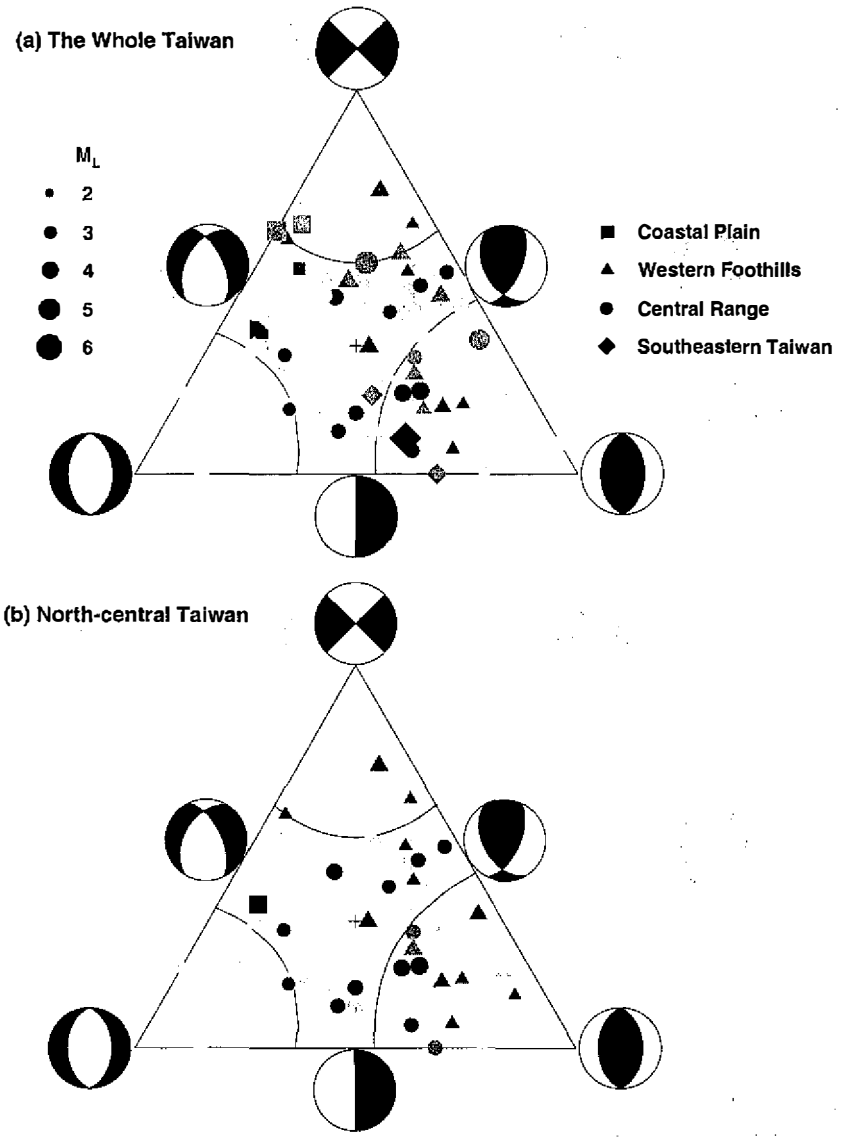

Fig. 5. Distribution of faulting on the triangle diagrams. (a) 97 events for whole of Taiwan, (b) 54 events for north-central Taiwan, (c) 33 events for south-central Taiwan, (d) 10 events for southeastern Taiwan.

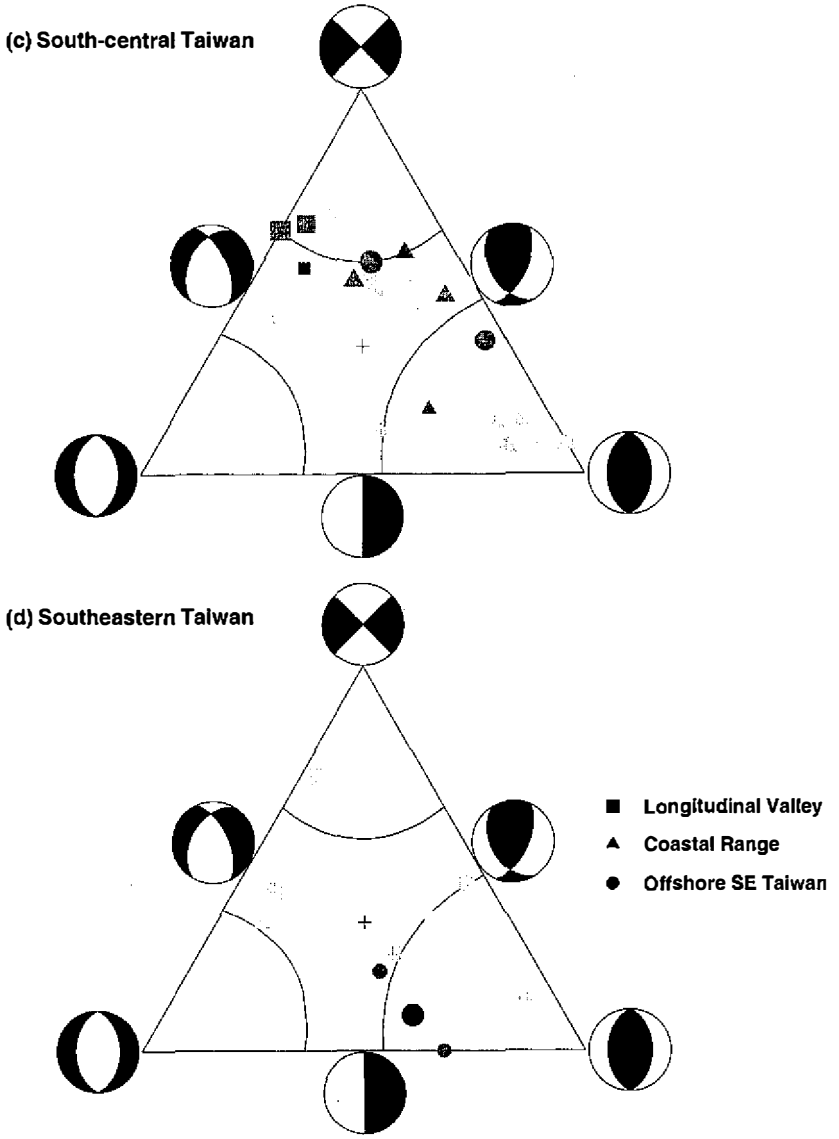

(*Fig. 5.* continued)

In the Western Foothills (elevation < 500 m), along the flank of the Central Range, two forms of deformation are observed. One is dominated mainly by normal faulting at shallow depths (~ 13 km; A40, A46-51), and the other one is characterized by reverse faulting at a depth range of 17-29 km (A2, A6-7, A26, A37). Most of these events occurred near the Chuchih fault, the boundary between the Western Foothills and the Hsuehshan Range. This fault is a reverse fault, dipping steeply to the east (Biq, 1971). From recent GPS measure-

ments, Yu *et al.* (1997) showed a considerable shortening across the fault. Coincidentally, the events with reverse motions predate those with normal motions that occurred at shallower depths.

3.3 South-central Taiwan

There are 33 focal mechanisms determined in south-central Taiwan, and all of them have a focal depth shallower than 22 km (Figure 4b). The focal mechanisms of most events in this area have an E-W striking P-axis and a N-S trending T-axis (Figure 6c). No normal faulting mechanism were located on the ternary diagram for this area (Figure 5c). About half of the events have odd mechanisms and the other half are split quite evenly between the strike-slip and reverse faulting regimes. In contrast to the events that occurred in the north, the events that occurred in the southern Central Range all contain strike-slip motion and occurred near the Chaochow fault - a steep east-dipping fault (Biq, 1971). In this area three events have M_L > 5 with either reverse (B21) or strike-slip (B29-30) faulting mechanisms. In southwestern Taiwan, three events (B15-17) show strike-slip faulting motions.

3.4 Southeastern Taiwan

As one can see in Figure 2, earthquakes in southeastern Taiwan do not occur less frequently than those in the interior of Taiwan. However, since most events located here do not have good station coverage, only 10 events met the event selection criteria used by Rau *et al.* (1996) and therefore only these are given in this paper (Figure 4c). In the southeastern Coastal Range, reverse and odd mechanisms as classified by the ternary diagram (Figure 5d) are observed. Farther to the south, in the southern Longitudinal Valley, reverse and strike-slip faulting occurred. For these Longitudinal Valley strike-slip events, if the N-S striking nodal planes are the fault planes, then they are left-lateral motions, which correspond to the nature of the Longitudinal Valley fault. Three events in the SE offshore area show reverse and odd faulting mechanisms.

4. STRESS INVERSION

McKenzie (1969) demonstrated that the P and T axes derived from a single fault plane solution may vary significantly from the principal stress directions; in other words, the actual principal tectonic stress directions may not be properly represented by a single fault plane solution. However, by assuming that the stress in a small region is uniform and different faults may be activated, and that the motions along the faults are consistent with the regional stress, one can invert for the stress utilizing the focal mechanisms of a group of earthquakes in the region. A number of inversion techniques have been developed to determine regional stresses from populations of fault-slip data, whether slickensides or slip vectors (e.g., Angelier, 1979, 1984; Gephart and Forsyth, 1984; Gephart, 1990a, b; Michael, 1984, 1987). These various techniques differ in their descriptions of misfit, normative measures of misfit, and approaches for locating the best stress model, but the underlying assumptions are similar. Among these techniques, the method from Gephart and Forsyth (1984), contrary to others, allows us to

determine the orientation of the stress tensor by inverting focal mechanism data without prior knowledge of the fault plane.

In this study we use the "exact" method of Gephart and Forsyth (1984) to determine the best-fitting regional principal stress directions and magnitude (R) of the intermediate principal stress relative to the maximum and minimum stresses ($R = (\sigma_2-\sigma_1)/(\sigma_3-\sigma_1)$, where $\sigma_1>\sigma_2>\sigma_3$). The method assumes that the deviatoric stress tensor is uniform over the region of study and that the observed slip direction marks the shear stress direction on any fault plane (Bott, 1959). In the inversion scheme the best stress model is the one which predicts the fault geometry that is most consistent with all the observations. A grid search over a pre-specified range for the four parameters (three stress directions and R) of the stress model is employed to locate the best stress model. For each focal mechanism and each stress model, a misfit is determined. The misfit is defined as the smallest angle of rotation about any axis of general orientation that brings the observed focal mechanism into agreement with a predicted focal mechanism in which the slip vector matches the direction of resolved shear stress on one of the nodal planes. Each focal mechanism acquires two misfits, and the one with the smaller misfit is chosen as the fault plane. A measure of overall fitness of the model is obtained by summing the misfits of all the data. The best-fitting stress model is chosen to be the one having the smallest sum of misfits. Those models having the same value of sum of misfits, which are equally acceptable, can be mapped into confidence limits using the one-norm statistic (Gephart and Forsyth,1984; Parker and McNutt, 1980). In this study we computed the 95% confidence limits of the results.

4.1 Analysis of misfit as a function of fault plane solution errors

The meaning of the size of the misfit in the inversion technique is not well understood. Wyss *et al.* (1992) and Gillard and Wyss (1995) employed a series of synthetic tests and examined the size of the misfit, which may be due to errors in the fault plane solutions alone. Gillard and Wyss (1995) found that for random perturbations of fault plane solutions of up to 20°, the average error of σ_1 and σ_3 was less than 7°, and the misfits were less than 6°. For random perturbations of 30° and 40°, the misfits were larger than 7°, and the errors of σ_1 and σ_3 were 11° and 23°, respectively. Thus only inversion results with misfits smaller than 6° were accepted as representing data from volumes with an approximately homogeneous stress tensor orientation. Similar results were also obtained by Wyss *et al.* (1992). Furthermore, Gillard and Wyss (1995) pointed out that the result of the synthetic test may depend on the nature of the data set itself, and they suggested that the error analysis should be done every time a new stress inversion study is undertaken.

Following the approach of Gillard and Wyss (1995), we chose a data set of 33 focal mechanisms in south-central Taiwan (Figure 4b) to generate the synthetic data set. The synthetic data were generated by adjusting the 33 focal mechanisms such that the slip vector on one of the nodal planes coincided with the predicted slip direction on that plane. We then perturbed the strike, dip, and rake of each focal mechanism in the synthetic data by adding random errors in normal (Gaussian) distributions with standard deviations of 5°, 10°, 15°, 20°, 30°, and 40°, respectively. From the results of synthetic tests (Table 2), we found that for

errors $\leq 10°$ that could be expected in a data set of focal mechanisms, the average misfits are $< 7°$, and the stress orientations remain unchanged. When the error is 15°, the average misfit is 8.4°, and the average error of stress orientations deviates 4° from the "error free" ones. For fault plane solution errors $\geq 20°$, the average misfits are $> 9.6°$ and the error free stress orientations are recovered poorly with an average error $> 30°$. Thus, we propose that for inversion results with average misfits $< 9°$, the data sets are likely to have come from a volume where the stress state is homogeneous. However, if the average misfits are $> 9°$ for the inversion results, the data sets may indicate a heterogeneous stress field.

5. STATE OF STRESS IN DIFFERENT REGIONS

5.1 The Whole of Taiwan

We first inverted the data set containing all 97 events. The inversion gave a relatively large spread of the 95% confidence region for σ_1 and σ_3, a broad distribution of R values, and a best-fitting stress model with an average misfit of 11.2° (Figure 6a). The spread of R values and the misfit are too large to be acceptable by the standard set by our error analysis, which indicates that the whole region studied is not homogeneous. Nevertheless, the orientations of the stress tensor are fairly well constrained with σ_1 and σ_3 striking in the directions centered at about 289° and 196°. The best-fitting stress models for the whole of Taiwan and the subsets investigated below are shown in Table 3. Below we will examine the data set from each subset and investigate if the state of stress derived for the subsets is more uniform than that of the whole of Taiwan.

5.2 North-central Taiwan

In comparison with the result for the whole of Taiwan, the inversion for the north-central Taiwan data set (54 events) gives an even larger spread of the 95% confidence region for σ_1 and σ_3 and a broader distribution for R values (Figure 6b). The best-fitting stress model for this inversion has an average misfit of 11.3°, and it indicates that the stress field inverted from

Table 2. Relationship between fault plane solution errors and misfit for synthetic data.

Fault plane solution errors (°)	Misfit (°)	Average error of σ_1 and σ_3 (°)
0	0.211	0
5	3.293	0
10	6.956	0
15	8.407	4
20	9.644	32
30	9.631	30
40	11.055	37

this data set is not homogeneous. The optimal σ_1 and σ_3 directions strike in the directions of 316° and 199°, respectively. Although this data set contains a relatively large number of events, there is no noticeable tectonic or seismicity separation which may divide this data set into different subsets.

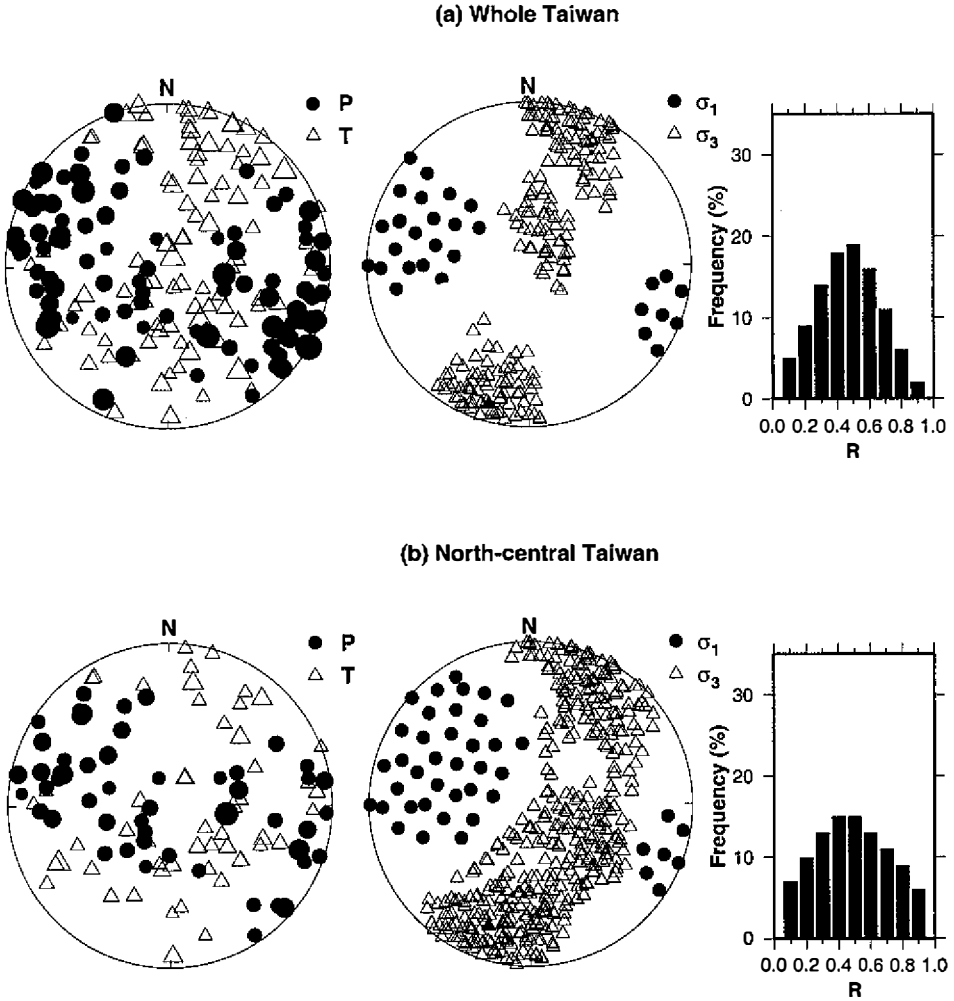

Fig. 6. Results of stress inversions. (Left column) Lower hemisphere projection of P (dark circles) and T (white triangles) axes. (Middle column) 95% confidence region for σ_1(dark circles) and σ_3 (white triangles) plotted on a lower hemisphere stereographic projection. (Right column) Distribution of R values for stress models within 95% confidence region. (a) whole of Taiwan, (b) north-central Taiwan, (c) south-central Taiwan, (d) southeastern Taiwan.

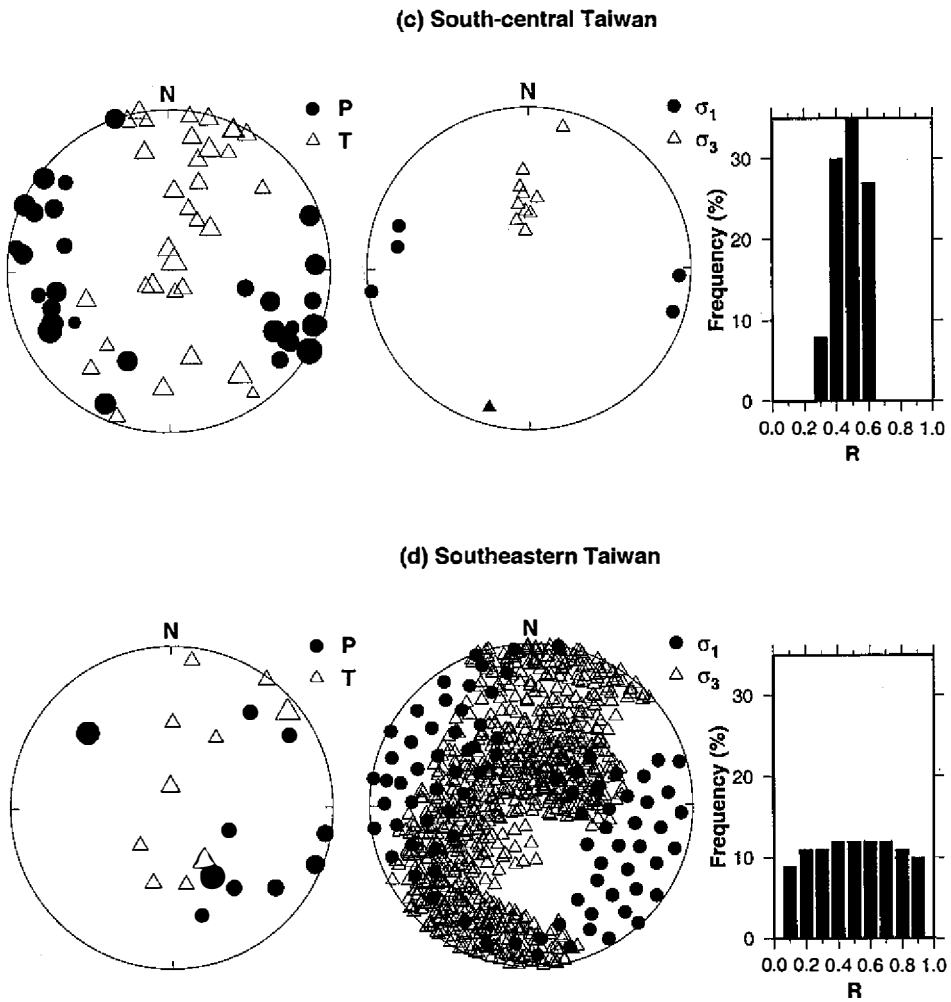

(*Fig. 6.* continued)

5.3 South-central Taiwan

33 events were used in this data set. The stress model inverted for south-central Taiwan shows considerably well constrained 95% confidence limits for σ_3 and σ_1, and a narrow range of R values (Figure 6c). The best-fitting stress model has an average misfit of 5.3° indicating that the stress field is nearly homogeneous in this area. The optimal σ_1 and σ_3 directions are horizontal and sub-horizontal striking in the directions of 93° and 351°, respectively.

5.4 Southeastern Taiwan

There are only 10 events available in this data set. As expected, the result of the inversion shows a large spread of 95% confidence limits for σ_3 and σ_1 (Figure 6d). The average misfit

Table 3. Stess tensor directions estimated from focal mechanism solutions in different regions.

area	σ_1 (°) (pl, az)	σ_2 (°) (pl, az)	σ_3 (°) (pl, az)	R	Ave. misfit (°)
whole Taiwan	17, 289	69, 73	12, 196	0.5	11.169
n-c Taiwan	48, 316	34, 93	22, 199	0.6	11.310
southern Taiwan	8, 93	32, 188	57, 351	0.5	5.262
southeastern T.	2, 298	27, 206	62, 32	0.2	6.072

for the best-fitting stress model is low (6.1°) and this is a result of the small number of data used.

6. DISCUSSION

The study of earthquake focal mechanisms allows us to view the geometry and orientations of the faults at the time of movement. Combining the focal mechanism data with the longer-term geological record, it is possible to reconstruct the tectonic process of a region through time. In this study, although the observed mechanisms of the minor earthquakes are rather diverse, and over time, the focal mechanism distribution may vary, we do see some intriguing patterns already. For the 97 events, reverse faulting is mainly observed in the Western Foothills, with P-axes trending NNW-SSE or E-W. Strike-slip faulting is seen mainly in the southern Central Range and the Western Foothills with P axes trending NNW-SSE or NW-SE and T axes trending NNE-SSW or NE-SW. Normal faulting is observed mainly in the northern Central Range with several different directions of T-axes trending. Thus, a certain degree of regionalization of focal mechanisms can be seen in the Taiwan orogen.

Yeh *et al.* (1991) compiled a heterogeneous set of pre-1987 focal mechanisms and determined the stresses in various areas in Taiwan. The events used range in magnitude from about 2 to greater than 7, and the dataset includes a large number of events offshore from Taiwan. It is quite clear in both studies that normal faulting dominates in northern Taiwan. But while the results of Yeh *et al.* (1991) show a mixture of normal, reverse, and strike-slip faulting in the Western Foothills of southwestern Taiwan (23°N and 120.7°E), Figure 4b indicates an absence of normal faulting in this region. Such differences may be a result of the relatively short time period covered in this study.

Yu *et al.* (1997) reported velocity field results from GPS measurements in Taiwan. They showed that while NW-oriented compressive strain dominates in the Coastal Range, the Longitudinal Valley and in the Western Foothills, the southern Central Range is dominated by NEE-oriented extension. These observations were made on the surface and do not necessarily agree with the mode of deformation at depth. For instance, although few focal mechanism solutions were obtained under the southern Central Range (Figure 4b), no normal faulting corresponds to the extension indicated by the GPS measurements. However, the mostly reverse faulting under the Western Foothills coincides with the GPS observations.

The Taiwan orogen is frequently mentioned as a typical example of the thin-skinned tectonic model (e.g., Suppe, 1981). In the thin-skinned model, the deformation of the orogenic belt is dominated by slip on thrust faults and related fault-bend folding within a wedge-shaped zone above a basal decollement. Furthermore, this model assumes that the upper and lower crust of the orogen are decoupled and it does not address deep-seated deformation. In this study, for the 30 reverse events in the Taiwan orogen, only 3 of them have a depth shallower than 10 km, while the other 27 are located in the mid- and lower-crustal levels. Most of these events have nodal planes dipping at high angles (> 30°), and only 4 of them are probably low-angle faults (< 20°; Figure 4). These mostly steeply dipping nodal planes and the depths of these reverse faulting earthquakes show that reverse faulting in the Taiwan orogen is not confined above the assumed shallow detachment surface but occurs in the crystalline basement at high angles.

In a compressive orogeny, reverse faulting is generally the dominant mode of deformation, but the completely opposite mechanism, normal faulting, is also commonly recognized within the orogen (e.g., Dewey, 1988; England and Molnar, 1993). Based on structural analyses in the north-central Central Range (Crespi *et al.*, 1996), extension seems to be a common form of deformation in some parts of the Central Range. Based on our results, active normal faulting is taking place in the northern portion of the Central Range at both the shallow (< 14 km) and deep (31-36 km) levels. The shallow normal faulting may be related to the uparching of the core of the orogen (Rau and Wu, 1995), which causes extension in the outer portion of the core. This motion results in a vertical stress greater under the orogen than in adjacent areas. On the other hand, the finding of deep normal faulting under the Central Range is certainly not new, and the cause of the deep normal faulting is rather intriguing. Lin and Roecker (1993) studied the seismicity (1975-1984) and focal mechanisms in an area of about 20 x 110 km^2 near 24°N, and they found 11 normal faulting out of 29 solutions they obtained. The 11 events have a depth range of 30-65 km and M_L of 2-4. Lin and Roecker (1993) explained the normal faulting as the result of a pull from the deeper oceanic lithosphere that subducted prior to the collision on an increasingly buoyant and resistive continental crust entering the collision zone. This explanation requires the existence of the old, deeper subducted oceanic lithosphere, which is questioned by Rau (1992). Note that as the crust thickens, the thick, cold continental lithosphere can become gravitationally unstable and sink or delaminate (e.g., Bird, 1979; Houseman *et al.*, 1981; Platt and England, 1994). As the block of continental lithosphere (possibly including the lower crust) sinks into the mantle, it is replaced by hot asthenosphere mantle. To accommodate such a process, normal faulting occurs. This explanation is highly hypothetical; the available data do not allow this question to be answered.

At one location in the middle of the Western Foothills, the deeper (17-29 km) events (A2, A6-7, A26, A37) have consistent mechanisms with reverse faulting motions, while the shallow (~ 13 km) ones (A40, A46-51) have mechanisms with normal faulting motions. These are separated in both space and time. The reverse faulting events preceded the normal faulting events. These two may form a pair: compression in the lower crust and tension in the upper crust with σ_1 for the former and σ_3 for the latter in essentially the same direction. Note that these events occurred under the low-elevation (< 500 m) flank of the Central Range. Although

tension may be present mainly at high elevations, while the interior of the orogen is under horizontal compression, normal faulting can still occur on the flank of the orogen, resulting from the up-arching of the orogen. Apparently, normal faulting is a common form of deformation in the otherwise compressional Taiwan orogen. The normal faulting occurs in the high elevation region (northern Central Range), in a lower elevation area (Western Foothills) and in the Taiwan Strait (Kao and Wu, 1996). Although on a much smaller scale, the presence of normal faulting in Taiwan is similar to that in the Himalaya (e.g., Molnar and Tapponnier, 1978; Armijo *et al.*, 1986).

Two different styles of strike-slip faulting are identified in both east and south of the Peikang basement high area (Figure 4b). These cases of strike-slip faulting may result from the indentation of the Peikang basement high (e.g., Tapponnier *et al.*, 1986). Note that the number of strike-slip faulting events observed in this area from this study is rather small (a total of 9). As the focal mechanism solutions accumulate through time, they can be used to examine whether the Peikang basement high indeed acts as an indentor.

Previously, the stress tensors in the Taiwan area were constructed by Angelier *et al.* (1986, 1990) based on analyses of fault-slip data and by Yeh *et al.* (1991) based on focal mechanisms of 200 earthquakes prior to 1987. The stress pattern in western Taiwan based on their results was characterized by a fan-shaped distribution with σ_1 moving from NW-SE in the north to NE-SW in the south and σ_3 going from NE-SW in the north to NW-SE in the south. Although we did not attempt to divide our data set in the way Angelier *et al.* (1986) and Yeh *et al.* (1991) did, our stress inversion results are consistent with theirs where the areas overlap (Table 3). Most of the stress models we determined are poorly resolved and only one of them, the model in south-central Taiwan, is relatively well-determined. The wide range of "acceptable" solutions for most stress models may be due to the heterogeneous stress field and the small number of focal mechanisms used. Nevertheless, the best-fitting stress models in these areas are in agreement with the results of Angelier *et al.* (1986, 1990) and Yeh *et al.* (1991) and are consistent with the plate motion vectors in the vicinity of Taiwan (Seno *et al.*, 1993).

7. CONCLUSIONS

The focal mechanisms of small-to-moderate earthquakes in the Taiwan orogen are highly variable from area to area. Within a small area, the mechanisms are frequently similar, or, the mechanisms may be different, but they are consistent with a local stress tensor. Using diverse mechanisms, we investigated the nature of faulting in this region and examined the variations of stress tensors within the Taiwan orogen. Of the 30 reverse faulting events observed, 24 of them occurred under the Western Foothills and the Central Range, mostly within a depth range of 10-32 km and a dip angle range of 30-70°. The steeply dipping nodal planes and their deep (> 10 km) focal depths demonstrate that the reverse faulting is not confined above a detachment surface, but occurs in the crystalline basement at high angles. Normal faulting occurs in the high elevation region (northern Central Range), in a lower elevation area of the Western Foothills, and in the Taiwan Strait (Kao and Wu, 1996). Although on a much smaller scale, the normal faulting in Taiwan closely mimics that in the Himalaya. The stress tensors estimated are heterogeneous for the whole region and some of the subvolumes, with only the data

set for south-central Taiwan yielding a nearly homogeneous stress field. Although the spreads of the 95% confidence region for σ_1 and σ_3 are relatively large for most of the stress models, the best σ_1 and σ_3 models are consistent with the direction of the plate motion of the Philippine Sea plate relative to the Eurasian plate.

Acknowledgments We thank C.-S. Liu, J.-M. Chiu and two anonymous reviewers for careful reviews which improved the original manuscript. We also thank the staff of the Seismology Center of the Central Weather Bureau for providing high-quality earthquake data used in this research. This study was partially funded by US National Science Foundation (EAR-9206545 and INT-9513945), and the Institute of Earth Sciences, Academia Sinica in Taiwan.

REFERENCES

Angelier, J., 1979: Determination of the mean principal directions of stresses for a given fault population. *Tectonophysics,* 56, T17-T26.

Angelier, J., 1984: Tectonic analysis of fault slip data sets. *J. Geophys. Res.,* **89**, 5835-5848.

Angelier, J., E. Barrier, and H. T. Chu, 1986: Plate collision and paleostress trajectories in a fold-thrust belt: The foothills of Taiwan. *Tectonophysics,* **125**, 161-178.

Angelier, J., F. Bergerat, H. T. Chu, and T. Q. Lee, 1990: Tectonic analysis and the evolution of a curved collision belt: The Hsuehshan Range, northern Taiwan. *Tectonophysics,* **183**, 77-96.

Armijo, R., P. Tapponnier, J. L. Mercier, and T. Han, 1986: Quaternary extension in southern Tibet: Field observations and tectonic implications. *J. Geophys. Res.,* **91**, 13,803-13,872.

Biq, C., 1971: Some aspects of post-orogenic block tectonics in Taiwan - Recent crustal movements. *Royal Soc. New Zealand Bull.,* **9**, 19-24.

Bird, P., 1979: Continental delamination and the Colorado Plateau. *J. Geophys. Res.,* **84**, 7561-7571.

Bott, M. H. P., 1959: The mechanics of oblique slip faulting. *Geol. Mag.,* **96**, 109-117.

Chen, C. H., H. T. Chu, and T. Y. Chuang, 1983: Some structural problems of the Central Range of Taiwan (in Chinese with English abstract). *Bull. Central Geol. Surv.,* **2**, 1-16.

Clark, M. B., D. M. Fisher, C. Y. Lu, and C. H. Chen, 1993: Kinematic analyses of the Hsuehshan Range, Taiwan: A large-scale pop-up structure. *Tectonics,* **12**, 205-217.

Crespi, J., Y.-C. Chan, and M. S. Swaim, 1996: Synorogenic extension and exhumation of the Taiwan hinterland. *Geology,* **24**, 247-250.

Deffontaines, B, J. C. Lee, J. Angelier, J. Carvalho, and J.P. Rudant, 1994: New geomorphic data on the active Taiwan orogen: A multisource approach. *J. Geophys. Res.,* **99**, 20243-20266.

Dewey, J. F., 1988: Extensional collapse of orogens. *Tectonics,* **7**, 1123-1139.

England, P, and J. Jackson, 1989: Active deformation of the continents. *Ann. Rev. Earth Planet. Sci.,* **17**, 197-226.

England, P., and P. Molnar, 1993: Cause and effect among thrust and normal faulting, anatectic melting and exhumation in the Himalaya. Himalayan Tectonics. In: P. J. Treloar and

M. P. Searle (Eds.), Geol. Soc. Spec. Publ. Lond., 401-411.

Frohlich, C., 1992: Triangle diagrams: ternary graphs to display similarity and diversity of earthquake focal mechanisms. *Phys. Earth Planet. Inter.*, **75**, 193-198.

Frohlich, C., 1995: Cliff's nodes concerning plotting nodal lines for P, S_h and S_v, Univ. Texas Inst. Geophysics Technical Report No. 132, 29 pp.

Frohlich, C., and K. D. Apperson, 1992: Earthquake focal mechanisms, moment tensors, and the consistency of seismic activity near plate boundaries. *Tectonics,* **11**, 279-296.

Gephart, J. W., FMSI: 1990a: A Fortran program for inverting fault/slickenside and earthquake focal mechanism data to obtain the regional stress tensor. *Comput. and Geosci.,* **16**, 953-989.

Gephart, J. W., 1990b: Stress and the direction of slip on fault planes. *Tectonics,* **9**, 845-858.

Gephart, J. W., and D. W. Forsyth, 1984: An improved method for determining the regional stress tensor using earthquake focal mechanism data: application to the San Fernando earthquake sequence. *J. Geophys. Res.*, **89**, 9305-9320.

Gillard, D., and M. Wyss, 1995: Comparison of strain and stress tensor orientation: Application to Iran and southern California. *J. Geophys. Res.*, **100**, 22,197-22,213.

Ho, C. S., 1988: An introduction to the geology of Taiwan: Explanatory text of the geologic map of Taiwan, Min. of Econ. Aff., Taipei, Taiwan, Republic of China, 192 pp.

Houseman, G. A., D. P. McKenzie, and P. Molnar, 1981: Convective instability of a thickened boundary layer and its relevance for the thermal evolution of continental convergence belts. *J. Geophys. Res.*, **86**, 6115-6132.

Kao, H., S. J. Shen, and K.-F. Ma, 1998: Transition from oblique subduction to collision: Earthquakes in the southernmost Ryukyu arc-Taiwan region. *J. Geophys. Res.*, **103**, 7211-7229.

Kao, H., and F. T. Wu, 1996: The September 16, 1994 earthquake (m_b = 6.5) in the Taiwan Strait and its tectonic implications. *TAO,* **7**, 13-30.

Kikuchi, M., and H. Kanamori, 1982: Inversion of complex body waves, *Bull. Seism. Soc. Am.,* **72**, 491-506.

Lee, J.-C., J. Angelier, and H.-T. Chu, 1997: Polyphase history and kinematics of a complex major fault zone in the northern Taiwan mountain belt: the Lishan Fault. *Tectonophysics,* **274**, 97-115.

Lee, T. Q., 1983: Focal mechanism solution and their tectonic implications in Taiwan region. *Bull. Inst. Earth Sci. Acad. Sin.,* **3**, 37-54.

Lin, C. H., and S. W. Roecker, 1993: Deep earthquakes beneath central Taiwan: mantle shearing in an arc-continent collision. *Tectonics,* **12**, 745-755.

Lin, M. T., and Y. B. Tsai, 1981: Seismotectonics in Taiwan-Luzon area. *Bull. Inst. Earth Sci. Acad. Sin.,* **1**, 51-82.

McKenzie, D. P., 1969: The relation between fault plane solutions and the directions of the principal stresses. *Bull. Seism. Soc. Am.,* **59**, 591-601.

Michael, A. J., 1984: Determination of stress from slip data: Faults and folds. *J. Geophys. Res.*, **89**, 11,517-11,526.

Michael, A. J., 1987: Use of focal mechanisms to determine stress: A control study. *J. Geophys.*

Res., **92**, 357-368.

Molnar, P., and P. Tapponnier, 1978: Active tectonics of Tibet. *J. Geophys. Res.*, **83**, 5361-5375.

Parker, R. L., and M. K. McNutt, 1980: Statistics for the one norm misfit measure. *J. Geophys. Res.*, **85**, 4429-4430.

Platt, J. P., and P. C. England, 1994: Convective removal of lithosphere beneath mountain belts: thermal and mechanical consequences. *Am. J. Sci.*, **294**, 307-336.

Rau, R.-J., 1992: Flexure modeling and Taiwan tectonics, Master's thesis, State University of New York at Binghamton, 131 pp.

Rau, R.-J., and F. T. Wu, 1995: Tomographic imaging of lithospheric structures under Taiwan. *Earth Planet. Sci. Lett.*, **133**, 517-532.

Rau, R.-J., F. T. Wu, and T. C. Shin, 1996: Regional network focal mechanism determination using 3-D velocity model and SH/P amplitude ratio. *Bull. Seism. Soc. Am.*, **86**, 1270-1283.

Seno, T., S. Stein, and A. E. Gripp, 1993: A model for the motion of the Philippine Sea plate consistent with NUVEL-1 and geological data. *J. Geophys. Res.* **98**, 17,941-17,948.

Shin, T. C., 1993: The calculation of local magnitude from the simulated Wood-Anderson seismograms of the short-period seismograms in the Taiwan area. *TAO*, **4**, 155-170.

Slemmons, D. B. and C. M. Depolo, 1986: Evaluation of active faulting and associated hazards. Active Tectonics. In: R. E. Wallace (Ed.), U. S. Geol. Surv. Menlo Park, California, 45-62.

Suppe, J., 1981: Mechanics of mountain building and metamorphism in Taiwan. *Mem. Geol. Soc. China*, **4**, 67-89.

Tapponnier, P., G. Pelzer, and R. Armijo, 1986: On the mechanism of collision between India and Asia. Collision Tectonics. In: M. P. Coward and A. C. Ries (Eds.), Spec. Publs. geol. Soc. Lond., 115-157.

Teng, L. S., Y. Wang, C. H. Tang, C. Y. Huang, T. C. Huang, M. S. Yu, and A. Ke, 1991: Tectonic aspects of the Paleogene depositional basin of northern Taiwan. *Proc. Geol. Soc. China*, **34**, 313-336.

Wang, J. H., 1989: The Taiwan Telemetered Seismographic Network. *Phys. Earth Planet. Inter.*, **58**, 9-18.

Wells, D. L. and K. J. Coppersmith, 1994: New empirical relationships among magnitude, rupture length, rupture width, rupture area, and surface displacement. *Bull. Seism. Soc. Am.*, **84**, 974-1002.

Wu, F. T., 1978: Recent tectonics of Taiwan. *J. Phys. Earth*, **26**, Supp., S265-S299.

Wu, F. T., R.-J. Rau, and D. Salzberg, 1997: Taiwan orogeny: thin-skinned or lithospheric collision?. *Tectonophysics*, **274**, 191-220.

Wyss, M., B. Liang, W. R. Tanigawa, and X. Wu, 1992: Comparison of orientations of stress and strain tensors based on fault plane solutions in Kaoiki, Hawaii. *J. Geophys. Res.*, **97**, 4769-4790.

Yeh, Y. H., Barrier, E., C. H. Lin, and J. Angelier, 1991: Stress tensor analysis in the Taiwan area from focal mechanisms of earthquakes. *Tectonophysics*, **200**, 267-280.

Yu, S. B., H. Y. Chen, and L.-C. Kuo, 1997: Velocity field of GPS stations in the Taiwan area. *Tectonophysics,* **274,** 41-59.